RESEARCH ARTICLE

Brain Pathology

Protective role of Angiogenin in muscle regeneration in amyotrophic lateral sclerosis: Diagnostic and therapeutic implications

Paola Fabbrizio[1] | Sharada Baindoor[2] | Cassandra Margotta[1] | Junyi Su[3,4] |
Elena P. Morrissey[2] | Ina Woods[2] | Marion C. Hogg[2,6] | Sara Vianello[5] |
Morten T. Venø[3] | Jørgen Kjems[4] | Gianni Sorarù[5] | Caterina Bendotti[1] |
Jochen H. M. Prehn[2] | Giovanni Nardo[1]

[1]Laboratory of Neurobiology and Molecular Therapeutics, Department of Neuroscience, Istituto di Ricerche Farmacologiche Mario Negri IRCCS, Milano, Italy

[2]Department of Physiology and Medical Physics and SFI FutureNeuro Centre, Royal College of Surgeons in Ireland, Dublin, Ireland

[3]Omiics ApS, Aarhus, Denmark

[4]Interdisciplinary Nanoscience Center (iNANO) and Department of Molecular Biology and Genetics, Aarhus University, Aarhus, Denmark

[5]Department of Neuroscience, Azienda Ospedaliera di Padova, Padua, Italy

[6]School of Science and Technology, Nottingham Trent University, UK

Correspondence
Caterina Bendotti, Laboratory of Neurobiology and Molecular Therapeutics, Department of Neuroscience, Istituto di Ricerche Farmacologiche Mario Negri IRCCS, Via Mario Negri, 2, 20156 Milan, Italy.
Email: caterina.bendotti@marionegri.it

Jochen H. M. Prehn, Department of Physiology and Medical Physics and FutureNeuro SFI Research Centre, Royal College of Surgeons in Ireland, 123 St Stephen's Green, Dublin 2, Ireland.
Email: prehn@rcsi.ie

Funding information
Regione Lombardia, Grant/Award Number: CUP E48I20000000007; Science Foundation Ireland, Grant/Award Numbers: 17/JPND/3455, 20/SP/8953, 21/RC/10294_P2; EU Joint Programme-Neurodegenerative Disease Research; Ministero della Salute, Italy, Grant/Award Number: SG-2018-12366226; Agenzia di Ricerca per la Sclerosi Laterale Amiotrofica, Grant/Award Number: MUSALS-AChR; Science Foundation Ireland CRT in Genomics Data Science, Grant/Award Number: 18/CRT/6214

Abstract

Amyotrophic lateral sclerosis (ALS) is a fatal neuromuscular disease with no effective treatments, in part caused by variations in progression and the absence of biomarkers. Mice carrying the SOD1G93A transgene with different genetic backgrounds show variable disease rates, reflecting the diversity of patients. While extensive research has been done on the involvement of the central nervous system, the role of skeletal muscle remains underexplored. We examined the impact of angiogenin, including its RNase activity, in skeletal muscles of ALS mouse models and in biopsies from ALS patients. Elevated levels of angiogenin were found in slowly progressing mice but not in rapidly progressing mice, correlating with increased muscle regeneration and vascularisation. In patients, higher levels of angiogenin in skeletal muscles correlated with milder disease. Mechanistically, angiogenin promotes muscle regeneration and vascularisation through satellite cell-endothelial interactions during myogenesis and angiogenesis. Furthermore, specific angiogenin-derived tiRNAs were upregulated in slowly progressing mice, suggesting their role in mediating the effects of angiogenin. These findings highlight angiogenin and its tiRNAs as potential prognostic markers and therapeutic targets for ALS, offering avenues for patient stratification and interventions to mitigate disease progression by promoting muscle regeneration.

KEYWORDS
amyotrophic lateral sclerosis, Angiogenin, biomarkers, skeletal muscle, tiRNAs

1 | INTRODUCTION

Amyotrophic lateral sclerosis (ALS) is a lethal disease affecting motor neurons (MNs), marked by progressive degeneration in both upper and lower MNs [1]. Amyotrophic lateral sclerosis ranks among the most prevalent neuromuscular disorders globally, affecting all ethnic groups with an annual incidence of 2–3 per 100,000 individuals. Approximately 10% of cases are familial, linked to mutations in 12 distinct genes. The most commonly involved genes in ALS are SOD1, FUS, TARDBP, and C9ORF72. In contrast, the etiology of the remaining 90% of cases, which are sporadic, remains elusive [1]. Onset typically occurs in late middle life and presents as relentlessly progressive muscle atrophy and weakness. In most cases, the effects on respiratory muscles limit survival to 2–4 years after disease onset. Amyotrophic lateral sclerosis diagnosis is hindered by the absence of reliable biomarkers and primarily relies on clinical evaluation of symptoms, frequently resulting in delays exceeding 1 year from the onset of symptoms—potentially missing the optimal timeframe for disease-modifying treatments [2]. The remarkable clinical heterogeneity of the disease phenotype and course and the multisystemic nature of ALS pathology make identifying therapeutic targets challenging [2].

The denervation atrophy of skeletal muscles is an early event in the disease pathogenic cascade, anticipating ALS clinical symptoms [3]. Research using transgenic mSOD1 mice indicates that muscle wasting begins as early as 50 days postnatal, at a stage when there are no visible signs of degeneration in the spinal cord motor neurons [4]. The selective expression of mSOD1 in skeletal muscles results in denervation atrophy and MN loss, suggesting that skeletal muscle plays a crucial role as a therapeutic target in ALS [4]. These findings support the classification of ALS as a distal axonopathy, in which skeletal muscle is involved in a retrograde signalling pathway that leads to the deterioration of MNs [3].

Angiogenin (ANG) is a member of the vertebrate-specific RNase A family, which is widely expressed in most tissues and has been linked to angiogenesis, haematopoiesis, oncogenesis, inflammation, and immunity [5]. Angiogenin emerged as a significant player in ALS caused by the identification of loss-of-function mutations in the gene sequence of familial cases [6]. The identified mutations have been associated with an impairment in the angiogenic capacity of endothelial cells (ECs), suggesting a direct link between ANG dysfunction and aberrant vascular dynamics [6]. Angiogenin is also highly expressed by MNs, where it exerts a pivotal role in safeguarding viability by a multifaceted activity, including responses to excitotoxic and oxidative stress and control of protein homeostasis [7, 8]. Previous studies have shown that the systemic administration of recombinant human ANG (huANG) protein prevented MN death, improved vascularisation and increased lifespan in the SOD1G93A mouse model of ALS [7, 9]. Consistently, we demonstrated a higher expression of ANG mRNA and proteins in the MNs of SOD1G93A mice with slow- versus fast-progressing pathology [10]. Accumulating evidence indicates that the neuroprotective activity of ANG might be related to its RNase activity towards tRNAs with the production of tRNA-derived stress-induced RNAs (tiRNAs) [6, 11, 12]. 5' tiRNA may mediate the protective activities of ANG as they can inhibit global translation and promote stress granule (SG) assembly [13]. Furthermore, tiRNAs can interact with cytochrome c and protect cells from stress-induced apoptosis [14].

To evaluate whether the expression of ANG and tiRNA generation may also be a feature of peripheral tissues affected by ALS, in this study, we investigated ANG activity within the skeletal muscles of SOD1G93A mice. We found that ANG protein levels and ANG-derived tiRNAs were explicitly elevated in the skeletal muscle of slow-progressing mice compared to fast-progressing mice and correlated with increased vascularisation and myogenesis. Our results underscore the crucial role of ANG in the periphery as a prognostic index of ALS disease progression. These findings incentivise a deep exploration of ANG activity at a multisystem level to gain a comprehensive understanding of the associated pathogenetic mechanisms.

2 | MATERIALS AND METHODS

2.1 | Animals

This study utilised female transgenic SOD1G93A mice with genetic backgrounds of C57BL/6JOlaHsd (C57_SOD1G93A) and 129S2/Sv (129Sv_SOD1G93A), along with their corresponding non-transgenic (NTg) female littermates [10, 15, 16]. Procedures involving the animals and their care were conducted in accordance with the institutional guidelines of the Mario Negri Institute for Pharmacological Research, Milan, Italy (IRFMN).

2.2 | Tissue dissection and serum collection

Tibialis anterior (TA) was harvested from 129Sv_SOD1G93A and C57_SOD1G93A mice and their respective non-transgenic (NTg) littermates. The euthanasia was carried out at 12, 14, and 16 weeks of age for 129Sv_SOD1G93A mice and at 12, 14, 18, and 22 weeks of age for C57_SOD1G93A mice. These time points corresponded to the presymptomatic (PS; C57: 12, 14 wks, 129Sv: 12 wks), symptom onset (OS; C57: 18 wks, 129Sv: 14 wks), and symptomatic (SYMPT; C57: 22 wks, 129Sv: 16 wks) stages, determined based on their performance in the grip strength test [15, 16]. After euthanisation, muscles were excised from each mouse, rapidly

frozen in isopentane, chilled with liquid nitrogen, and preserved at $-80°C$. Subsequently, the muscles were weighed and employed in immunohistochemical, biochemical, and biomolecular analyses. At the age corresponding to the disease onset, blood from transgenic fast and slow mice and relative NTg was collected in EDTA pre-coated tubes (BD VacutainerK2EDTA), and serum was isolated from EDTA blood by centrifugation at $12,000\times$ g for 10 min at 18–20°C.

2.3 | RNA isolation

RNA was extracted from skeletal muscles using the Qiagen miRNeasy kit (Qiagen) and a tissue homogeniser, following the manufacturer's protocols, and eluted in 40 μL water containing 1 μL RNaseOUT RNase inhibitor (ThermoFisher). The concentration of RNA was determined using a Nanodrop. From serum, RNA was extracted using the Qiagen serum/plasma miRNeasy kit, incorporating 3.5 μL of Caenorhabditis elegans microRNA (miRNA)-39 spike-in (at a concentration of 1.6×10^8 copies/mL) during the extraction process as recommended by Qiagen. The RNA was then eluted in 20 μL of water with 1 μL RNaseOUT RNase inhibitor included.

2.4 | RNAseq

Prior to library preparation, RNA samples were treated with the demethylase AlkB. For each sample 1 μg total RNA was prepared in the reaction buffer with 80 pmol purified AlkB in a total volume of 100 μL. The reaction buffer contained 300 mM KCl, 2 mM MgCl2, 50 μM $(NH4)2Fe(SO4)2·6H2O$, 300 μM 2-ketoglutarate (2-KG), 2 mM l-ascorbic acid, 50 μg/mL BSA, 50 mM MES buffer (pH 5.0). The reaction was incubated for 4 h at room temperature and quenched with 5 mM EDTA. Then, the treated RNA was recovered by RNA Clean & Concentrator Kits (Zymo Research R1013). RNA samples from SOD1G93A and non-transgenic control mice were prepared for small RNA sequencing using NEBNext® Small RNA Library Prep kit (NEB). For all library preparations, a Pippin Prep (Sage Science) was used for size selection, allowing the library prepared from RNA up to 50 nt in length. This represents a larger than standard upper limit for small RNA sequencing and is done to allow improved sequencing of tiRNAs. The finished libraries were quality-controlled using an Agilent Bioanalyzer 2100. Libraries were sequenced on an Illumina sequencer.

2.5 | Biostatistics analysis

The Nextflow-based bioinformatics pipeline tsRNA-search with the species specified as mouse for identifying differentially expressed tsRNA was used [17]. The pipeline utilises Trim Galore for adapter removal with a minimum overlap of 10 bp with the adapter sequence. Reads shorter than 16 bp after removing the adapter sequence were discarded. It then maps the reads to a custom ncRNA database using STAR and generates the read counts using FeatureCounts. The pipeline implements a combination of five methods, namely distribution score, cleavage score, slope score, t-test (referred to as Fisher's method in the pipeline) and DESeq2 to identify the top differentially expressed tsRNAs. To reduce false positives, we selected tsRNAs with distinct cleavage plots and set an FC cutoff of 1.2 and a p-value cutoff of 0.05.

2.6 | Human skeletal muscle biopsies

Biopsies of human skeletal muscle were chosen from the Neuromuscular Bank of Tissues at the University of Padua, specifically from the Telethon Network of Genetic Biobanks (TNGB). The samples were rapidly frozen in the liquid phase of isopentane, pre-cooled in liquid nitrogen, for a duration not exceeding 45 s. Subsequently, the frozen muscles were preserved at –80°C until required. The progression rate of ALS was determined using the monthly ALS Functional Rating Scale-Revised (ALSFRS-R) slope, calculated as the progression rate to the last visit (PRL) defined by the formula 48-ALSFRS-R score at the last visit divided by the disease duration from onset to the last visit [18]. This parameter, denoted as ΔFS, was utilised to characterise the rate of disease progression in ALS patients. Clinical information regarding the ALS patients from whom the biopsies in this study were obtained can be found in Supplementary Table 1.

2.7 | Immunohistochemistry

Mice: 12 μm coronal serial muscle cryo-sections were collected on poly-lysine objective slides (VWR International, Milan, Italy) and kept at −20°C until use, when sections were fixed in acetone for 10′, air-dried, and washed. To determine ANG tissue location, the following primary antibodies were used: mouse anti-Pax7 (1:14; Abcam 528,428), rat anti-CD31 (1:300; BD Bioscience 550,274) and rabbit anti-Angiogenin (1:100; Santa Cruz Biotechnology 74,528), DAPI (1:500; Invitrogen), and respective secondary antibody: anti-mouse Alexa-flour 594, anti-rat Alexa Flour 488, anti-rabbit Alexa-flour 647 (1:500; Invitrogen) and. To evaluate muscle vascularisation rat anti-CD31 (1:300; BD Bioscience 550,274) followed by respective secondary antibody anti-rabbit Alexa-flour 647 (1:500; Invitrogen), and DAPI (1:500; Invitrogen). To determine embryonic muscle fibres, anti-MyH3 (1:10; DSHB F1652) and respective secondary antibody anti-MIgM Alexa-flour 647 (1:500; Invitrogen A21046) and WGA (1:500 Alexa-flour 488; Invitrogen W6748).

Imaging was performed using a sequential scanning mode on an A1 Nikon confocal equipped with NIS-Elements at 20× magnification. Embryonic myofibres were examined on muscle sections utilising the "MuscleJ" plug-in in Fiji (Image J, U. S. National Institutes of Health, Bethesda, Maryland), as previously described [16] CD31 analysis was performed evaluating the percentage of the area covered by the immunostaining (% Area Fraction) on coronal TA muscle sections through Fiji (Image J, U. S. National Institutes of Health, Bethesda, Maryland).

Humans: 10 μm coronal serial muscle cryo-sections were collected on poly-lysine objective slides (VWR International, Milan, Italy) and kept at −20°C until use, when sections were fixed in acetone for 10′, air-dried, and washed. To determine ANG tissue location, the following primary antibodies were used: rat anti-CD31 (1:300; BD Bioscience 550,274) and rabbit anti-Angiogenin (1:100; Santa Cruz Biotechnology 74,528), DAPI (1:500; Invitrogen), and respective secondary antibody: anti-rat Alexa Flour 488 and anti-rabbit Alexa-flour 647 (1:500; Invitrogen). Imaging was performed using a sequential scanning mode on an A1 Nikon confocal equipped with NIS-Elements at 40× magnification.

2.8 | Real-time PCR

RNA was isolated from TA using TRIzol (Invitrogen) and purified with PureLink RNA columns (Life Technologies). The extracted RNA underwent DNase I treatment, followed by reverse transcription utilising the High-Capacity cDNA Reverse Transcription Kit (Life Technologies). Real-time PCR was conducted with the TaqMan Gene expression assay (Applied Biosystems), adhering to the manufacturer's instructions as previously described [16] The PCR reactions were carried out on cDNA specimens in triplicate, employing 1× Universal PCR Master Mix (Life Technologies) and a 1× mix containing specific receptor probes (Life Technologies).

Relative quantification was assessed by computing the ratio of the cycle threshold (Ct), where the signal exceeds a pre-set threshold in the logarithmic phase for the target gene compared to the reference gene β-actin (4310881E; Life Technologies). Average values from triplicates for each specimen were considered as separate data points for analysis using the $2^{-\Delta\Delta Ct}$ method. The specific probe utilised for this purpose targeted the nicotinic cholinergic receptor, gamma subunit (AChRγ) (CHRNG; Mm00437419_m1; Life Technologies).

2.9 | tiRNA validation by TaqMan PCR

tiRNAs were quantified on QuantStudio 5 PCR machine from Thermofisher. Custom small RNA Taqman assays (ThermoFisher Scientific) for 5'Lys CTT, 5'Gly CCC and 5'Val CAC were designed and optimised [11]. Assay IDs are available on request. To normalise the tiRNA levels, the $2^{-\Delta\Delta Ct}$ method was employed, using U6 snRNA as the reference gene. The samples were diluted in nuclease-free water to reach a final RNA concentration of 100 ng. 5 μL of RNA was used for the reverse transcription reaction according to TaqMan Small RNA Assay protocol (ThermoFisher). The reverse transcription reaction samples were subsequently diluted 1:10 with water. 1 μL of cDNA was used for the per qPCR reaction, the samples were performed in triplicate, and a no-template control was included for each assay.

2.10 | Western blotting

Equal quantities of total protein homogenates were applied to a polyacrylamide gel and subsequently transferred to a PVDF membrane (Millipore), following previously established methods [16]. Subsequently, the membranes were subjected to immunoblotting using primary antibodies, succeeded by HRP-conjugated secondary antibodies (Santa Cruz Biotechnology). The visualisation was achieved using Luminata Forte Western Chemiluminescent HRP Substrate (Millipore) on the Chemi-Doc XRS system (Bio-Rad). Immunoreactivity was normalised to GAPDH or the total protein loaded, which was detected using the Stain-Free imaging technology from Bio-Rad, which employs a polyacrylamide gel containing a trialone compound to induce fluorescence of proteins directly within the gel through photoactivation. The incorporation of the fluorophore facilitates the visualisation of total proteins in the gel and their subsequent transfer to a membrane during western blotting. The antibodies employed included mouse anti-Pax7 (1:1000; DSHB), rabbit anti-MyoD (1:1000; Proteintech), mouse anti-MyoG (1:130; DSHB), mouse anti-Angiogenin (1:500; Abcam), rabbit anti-hSOD1 (1:1000; StressMarq Biosciences), rabbit anti-G3BP1 (1:5000, Proteintech), mouse anti-phosphoSMAD2/3 (1:1000; Cell Signalling Technology Inc.). Immunoblot of human muscle biopsies was performed with the same protocol described above using the mouse anti-Angiogenin (1:500; Abcam) primary antibody.

For human biopsies, multiple membranes were analysed using the following methodology: (i) an internal standard (IS), consisting of a mixture of all samples involved in the experiment, was loaded onto each gel; (ii) membranes were processed simultaneously; (iii) the immunoreactivity for each sample was subsequently normalised against the immunoreactivity of the IS.

2.11 | Extraction of detergent-insoluble and soluble proteins

Mouse tissues were homogenised in 10 volumes(w/v) of buffer, 15mMTris–HCl, pH 7.6, 1mMDTT, 0.25Msucrose,

1 mM MgCl2, 2.5 mM EDTA, 1 mM EGTA, 0.25 M sodium orthovanadate, 2 mM sodium pyrophosphate, 25 mM NaF, 5 mM MG132, and protease inhibitors cocktail (Roche; 1 tablet/ 10 mL), as previously described [19]. The method for isolating the Triton-resistant fraction from cell pellets was adapted according to previously established protocols [19]. Samples were first centrifuged at 10000 g at 4 °C for 15 min, with the initial supernatant collected into a new tube. The remaining pellet was resuspended in an ice-cold homogenisation buffer with 2% Triton TM X-100 and 150 mM KCl, then sonicated and agitated for 1 h at 4 °C. A second centrifugation was performed twice at 10000 g for 10 min to separate the Triton-resistant fraction (pellet) and produce a second supernatant. The two supernatants were combined to create the Triton-soluble fraction, which was subsequently analysed by western blot. The Triton-resistant pellet was resolubilised in either 7 M urea, 2 M thiourea, and 4% CHAPS, or in 50 mM Tris–HCl pH 6.8, 1 mM DTT, and 2% SDS. Image acquisition and densitometry were done as described in the previous section.

2.12 | Primary satellite cell cultures and immunofluorescence

The protocol for isolating and labelling satellite cells was conducted in accordance with the procedures outlined in Fabbrizio et al. [20]. Briefly, hindlimb muscles from three-week-old mice were digested for 45 min at 37 °C using a solution of PBS with added Dispase II, Collagenase A, CaCl₂, MgCl₂, and DNase I. The resulting cell suspension was filtered, then stained with CD45/CD31/Ter119 phycoerythrin (PE), Sca1-FITC, and α7 integrin allophycocyanin (APC) for sorting satellite cells (SCs). Sorted SCs with Moflo Astrios (Beckman Coulter, Brea, CA) were cultured on Matrigel-coated plates in Cyto-Grow complete medium and expanded until confluent. For myogenic differentiation, the medium was switched to DMEM with 2% horse serum for 48 h. Both proliferating and differentiating cells were treated with 100 ng/mL Angiogenin (Peprotech, London UK) for 24 h.

Satellite cell proliferation was assessed for each well based on image fields captured with an Olympus virtual slide system VS110 (Olympus, Tokyo, Japan), counting the number of DAPI+/Ki67+ (Anti-Ki67 Ab; Abcam) cells per field. Myogenic differentiation was assessed using five random pictures per condition as the per cent differentiation (no. of nuclei (DAPI+) in MyHC⁺ cells (1:20; DSHB) /total nuclei). Each well was analysed using a stereological random sampling approach for both procedures. A square grid of sample fields was overlaid on the image of each well using the "Grid" function to ensure an equal likelihood of sampling across the entire well. The analysis was based on the average of four image fields acquired at fixed distances from each other.

2.13 | C2C12 cell cultures

Murine C2C12 myoblasts were cultured in growth medium, specifically Dulbecco's modified Eagle's medium (DMEM) with heat-inactivated 10% fetal bovine serum (FBS), and 1% penicillin/streptomycin, at 37 °C under a humidified 5% CO_2 atmosphere. To induce differentiation from myoblasts to myotubes, the medium was switched to DMEM with 2% horse serum for 48 h. The cells were used for experiments between passages 3rd and 11th. Both proliferating and differentiating cells were treated with 10 ng/mL TGF-β1 (Peprotech, London, UK) and/or 100 ng/mL Angiogenin (Peprotech, London, UK) for 24 or 48 h.

2.14 | Statistics

Statistical analyses were conducted using GraphPad v.9.01 (GraphPad Software). Dependent variables and grouping variables were labelled on the y-axis and x-axis of the graphs, respectively. Data are expressed as mean ± SEM. Differences between two or more groups were assessed using parametric unpaired t-tests and Two-way ANOVA followed by Fisher's LSD test without correction. The D'Agostino & Pearson omnibus normality test and corresponding QQ plots evaluated the normality assumption. All experiments were performed at least three times unless specified otherwise. A significance threshold was set at $p < 0.05$. Detailed statistical results, including P values and sample sizes, are provided in the Results section, Figures, and associated captions. The correlation between ANG protein levels and disease progression in human muscle samples was analysed using the Spearman rank correlation coefficient.

3 | RESULTS

3.1 | The dynamic of skeletal muscle denervation atrophy discriminates the disease progression in ALS mice and is associated with differential ANG regulation

We analysed the denervation atrophy of hindlimb skeletal muscles (*Tibialis Anterior*, TA) in two SOD1G93A transgenic mice (C57BL6 and 129Sv), exhibiting a remarkable difference in the speed of symptom progression [15, 16]. Muscle mass reduction in the TA muscles of both fast and slow mice was compared to their respective non-transgenic (NTG) littermates across various ages corresponding to the presymptomatic (PS), Disease Onset (OS), and symptomatic (SYMPT) stages, as determined by performance on the grip strength test [16] and illustrated schematically in Figure 1A. TA muscle atrophy, quantified as the percentage of muscle loss in SOD1G93A mice relative to their respective NTG
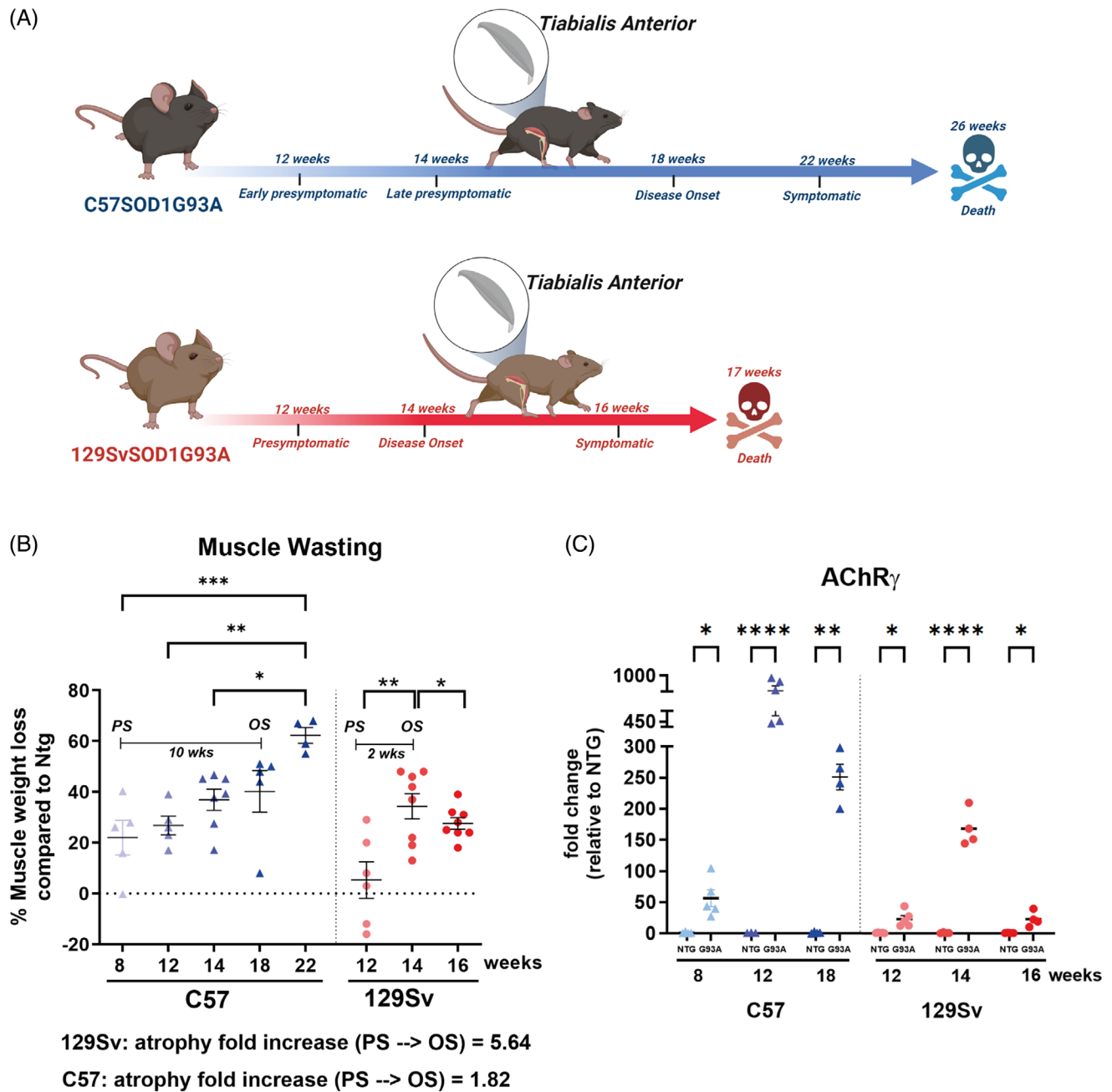
FIGURE 1 The dynamic of skeletal muscle denervation atrophy discriminates the disease progression in ALS mice. (A) Schematic representation of the disease progression in the two models of ALS. *Created with Biorender.com* (B) Muscle mass was calculated by measure of tibialis anterior (TA) muscles weight of 129SvSOD1G93A mice; C57SOD1G93A mice and NTg littermates at different time points of the disease. Percent muscle wasting was calculated relative to NTg mice at PS, OS and SY stage. Data are reported as mean ± SEM. Significance was calculated with 2-way ANOVA with uncorrected Fisher's LSD post-analysis (*$p \leq 0.05$, **$p \leq 0.01$; ***$p \leq 0.001$). (C) Real-time qPCR analysis of AChRγ mRNA transcripts in the TA of C57SOD1G93A and 129SvSOD1G93A mice compared with NTg littermates. Data are reported as mean ± SEM and expressed as fold change (%) of 129Sv NTg mice. Significance was calculated with Two-way ANOVA with uncorrected Fisher's LSD post-analysis (*$p \leq 0.05$, ****$p \leq 0.0001$).

littermates, exhibited distinct patterns across the different ALS mouse models. While abrupt muscle wasting occurred in fast-progressing mice (129Sv_SOD1G93A) in concomitance with symptom onset (OS; 14 weeks), mice with slow progression (C57_ SOD1G93A) showed moderate muscle atrophy at very early PS stage (8 weeks), keeping stable throughout disease

progression (early PS: 12 weeks, late PS: 14 weeks, OS: 18 weeks; SYMPT: 22 weeks). The rate of muscle wasting (measured as the fold change from PS to OS) increased by 5.6-fold in fast -progressing mice over 2 weeks (from 12 to 14 weeks) while in slow progressing mice, it increased only by 1.8-fold over 10 weeks (from 8 to 18 weeks) (Figure 1B). In line with muscle
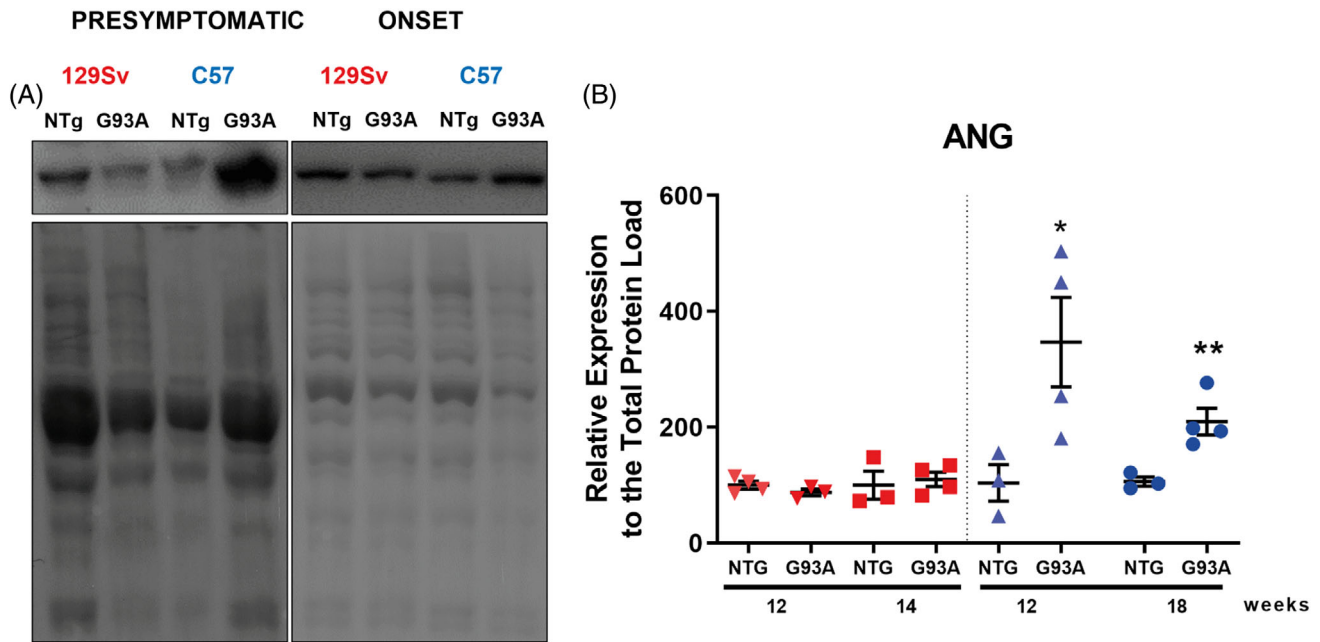
FIGURE 2 Disease progression in ALS mice is associated with differential ANG regulation. (A, B) Representative immunoblot images and relative densitometric analysis of Angiogenin protein expression in TA muscles of C57SOD1G93A and 129SvSOD1G93A mice compared with NTg littermates. Protein levels were normalised on the total amount of protein loaded. Data are reported as mean ± SEM. Significance was calculated with Two-way ANOVA with uncorrected Fisher's LSD post-analysis (*$p \leq 0.05$, **$p \leq 0.01$).

atrophy, there was a notable decrease in muscle innervation in mice with slow disease progression at both the presymptomatic (PS) and onset (OS) stages, as determined by the analysis of AChRγ mRNA levels, an indicator of endplate denervation [16], while in fast-progressing mice manifest denervation was found at the OS (Figure 1C). Notably, both slow and fast progressing mice exhibited a dramatic reduction in AChRγ mRNA levels as the disease progresses. This result was expected as a consequence of reduced synaptic protein turnover primarily driven by the progressive absence of neural input, which diminishes the signals necessary for receptor expression, ultimately impairing neuromuscular junction stability and regeneration [21]. We next investigated ANG protein levels in the skeletal muscles of both fast and slow-progressing mice during disease progression. No ANG increase was registered in the skeletal muscles of fast-progressing mice at all the analysed timepoints (Figure 2A,B, Supplementary Figure 1a,b). Conversely, we found a trend to an increased expression of ANG protein within the TA of slow-progressing mice at 8 weeks (Supplementary Figure 1a,c), with a significant rise at 12 weeks and 18 weeks compared to NTg littermates (Figure 2A,B).

These data suggest that skeletal muscle denervation atrophy discriminated ALS mice with a differential disease progression. During this process, ANG levels rose in the skeletal muscles of slowly progressing animals. This event may constitute a compensatory mechanism for stabilising skeletal muscle mass during the first disease stages.

3.2 | Small non-coding RNAseq analysis shows higher Angiogenin-derived 5′tiRNAs in the skeletal muscle of slow than fast mice

We next performed small RNA-Seq of 15- to 50–nt–long RNAs from total RNA in the TA muscles of rapid and slow-progressing transgenic mice and respective non-transgenic (NTg) mice at the disease onset (C57-SOD1G93A: 18 weeks; 129Sv-SOD1G93A: 14 weeks). The data analysis showed an overall increase of tRNA fragmentation in the skeletal muscle of C57_SOD1G93A mice but not 129SvG93A mice, compared to the relative NTg littermates (Figure 3A).

tRNA can be cleaved by ANG in the anticodon loop to generate tiRNAs, or by other ribonucleases, including DICER to generate shorter tRNA fragments (3′ and 5′tRFs) [12]. Muscle profiling of specific tRNA fragments well discriminated fast and slow-progressing mice (Figure 3B,C). We found that 5′ ValCAC was the most represented tiRNA in the skeletal muscle of slow-progressing mice with a fold change (FC) ratio of 3.2 (log2FC = 1.91) with respect to NTg mice. Conversely, no significant variation was found in fast-progressing mice (Figure 3D,E). We also identified a significant increase in 5′GlyCCC (FC = 1.6; log2FC = 1.07) and 5′LysCTT (FC = 1.3; log2FC = 0.33) expression in C57-SOD1G93A mice skeletal muscle (Figure 3D,E). Noteworthy, 5′ LysCTT, but not 5′ GlyCCC, levels also rose in the serum (FC = 1.40; log2FC = 0.49) of slow progressing mice compared to NTg (Supplementary Figure 2a,b). TaqMan-based PCR analysis using primers
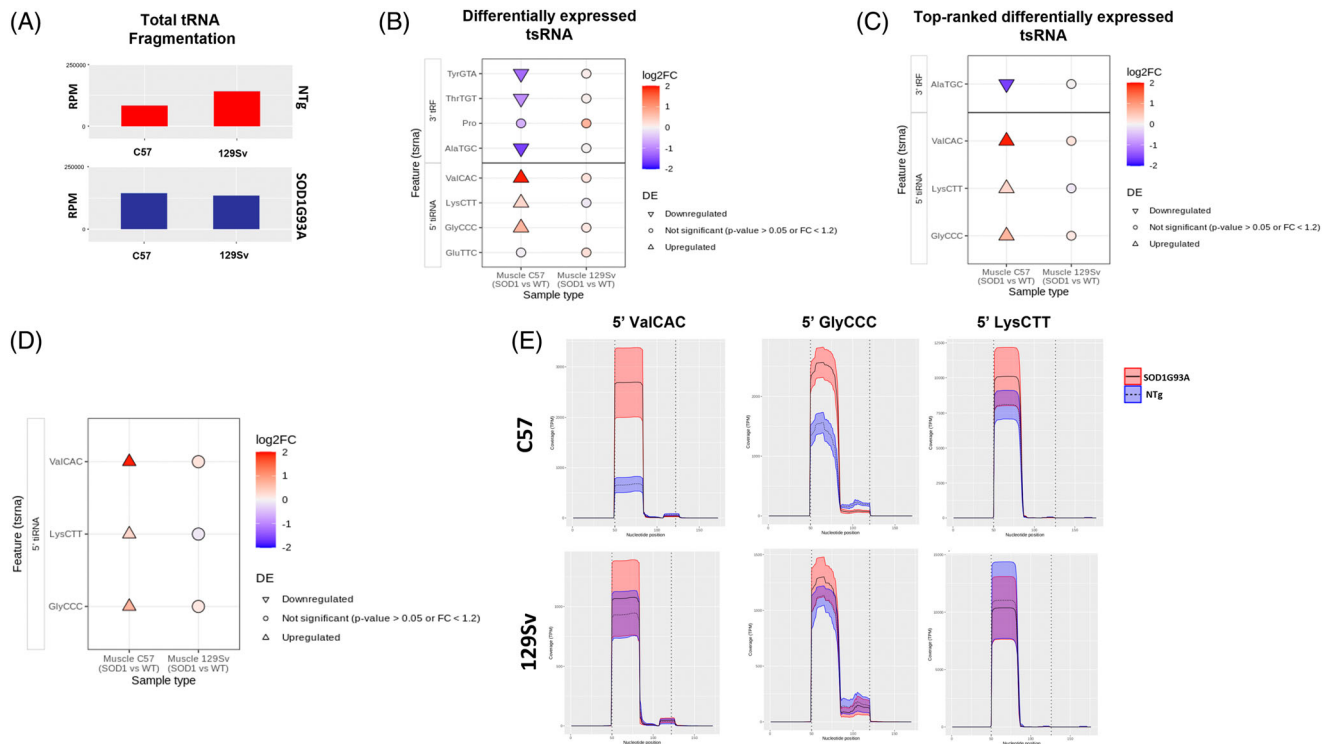
FIGURE 3 TsRNAs identified in RNA sequencing data from muscle tissue samples. (A) Normalised tRNA read counts identified in the NTg and SOD1G93A in C57 and 129Sv genetic backgrounds. (B) Summary of differentially expressed tsRNAs from the SOD1G93A versus NTg comparison in the C57 and 129Sv genetic background. The shape represents the regulation; upward facing arrow for upregulated, downward facing arrow for downregulated and a circle for not significant and the colour indicates the log2FC. (C) Summary of top differentially expressed tsRNAs with mean TPM greater than 100 from the SOD1G93A versus NTg comparison in the C57 and 129Sv genetic background. (D) Summary of top differentially expressed tiRNAs from the SOD1G93A versus NTg comparison in the C57 and 129Sv genetic background. (E) Coverage plots of 5′ ValCAC, 5′ GlyCCC, 5′ LysCTT tiRNAs identified as top differentially expressed tiRNAs. The x-axis represents the nucleotide position and the y-axis represents the coverage in TPM. The two vertical dotted lines enclose the main tRNA segment of 70 bp, with an additional 50 bp included both upstream and downstream. The dotted line illustrates the mean coverage for NTg samples, while the solid line represents the mean coverage for the SOD1G93A condition, with the shaded areas indicating the standard deviation for both conditions.

specifically detecting tiRNA halves [11] in whole muscle extract of fast and slow mice and relative NTg littermates validated the specific rise in the expression levels of the ANG-derived tiRNAs in C57-SOD1G93A (Supplementary Figure 3a–c). Notably, these variations are specific to the disease onset as the same validations performed at presymptomatic did not lead to significant differences for both fast and slow transgenic mice compared to their NTg littermates (Supplementary Figure 3d–f).

Stress granules assembly is a component of the ANG- and tiRNA-induced stress response programme in ALS and FTD. Accordingly, we evaluated if the rise in ANG-derived 5′ tiRNAs was associated with increased SG production in the skeletal muscle of slow-progressing mice. Biochemical analyses of SGs revealed that RNA-binding proteins within SGs, such as G3BP1, are insoluble in Triton or SDS, mirroring the biochemical properties of protein aggregates found in numerous neurodegenerative disorders [22]. Accordingly, we generate soluble (SOL) and triton insoluble (TIF) fractions of proteins from the skeletal muscles of fast and slow-progressing mice and relative NTg littermates at the disease onset to quantify G3BP1 and hSOD1 protein levels.

Results showed a significant and specific rise of G3BP1 in both SOL and TIF of skeletal muscle of slow mice (Figure 4A,B). This increase was unrelated to pathogenic SOD1 protein inclusion formation as these did not occur in skeletal muscles [23]. Indeed, unlike CNS [15], we found no human mutant SOD1 protein aggregation in muscle from both transgenic mouse models (Figure 4A–C). Accordingly, these results hint at a higher production of SGs in the skeletal muscle of slow mice than in fast mice, suggesting that similar to the CNS, ANG-RNase activity may be crucial in regulating cellular stress response and survival via stimulation of SG formation, even in skeletal muscle.

3.3 | Increased Angiogenin protein levels in the skeletal muscle of ALS mice correlate with enhanced muscle vascularisation and myogenesis

Skeletal muscle is richly vascularised, featuring a complex network of microvasculature interspersed among the myofibers. The regenerative process of muscle depends on the ability of SCs, which are the resident stem cells in
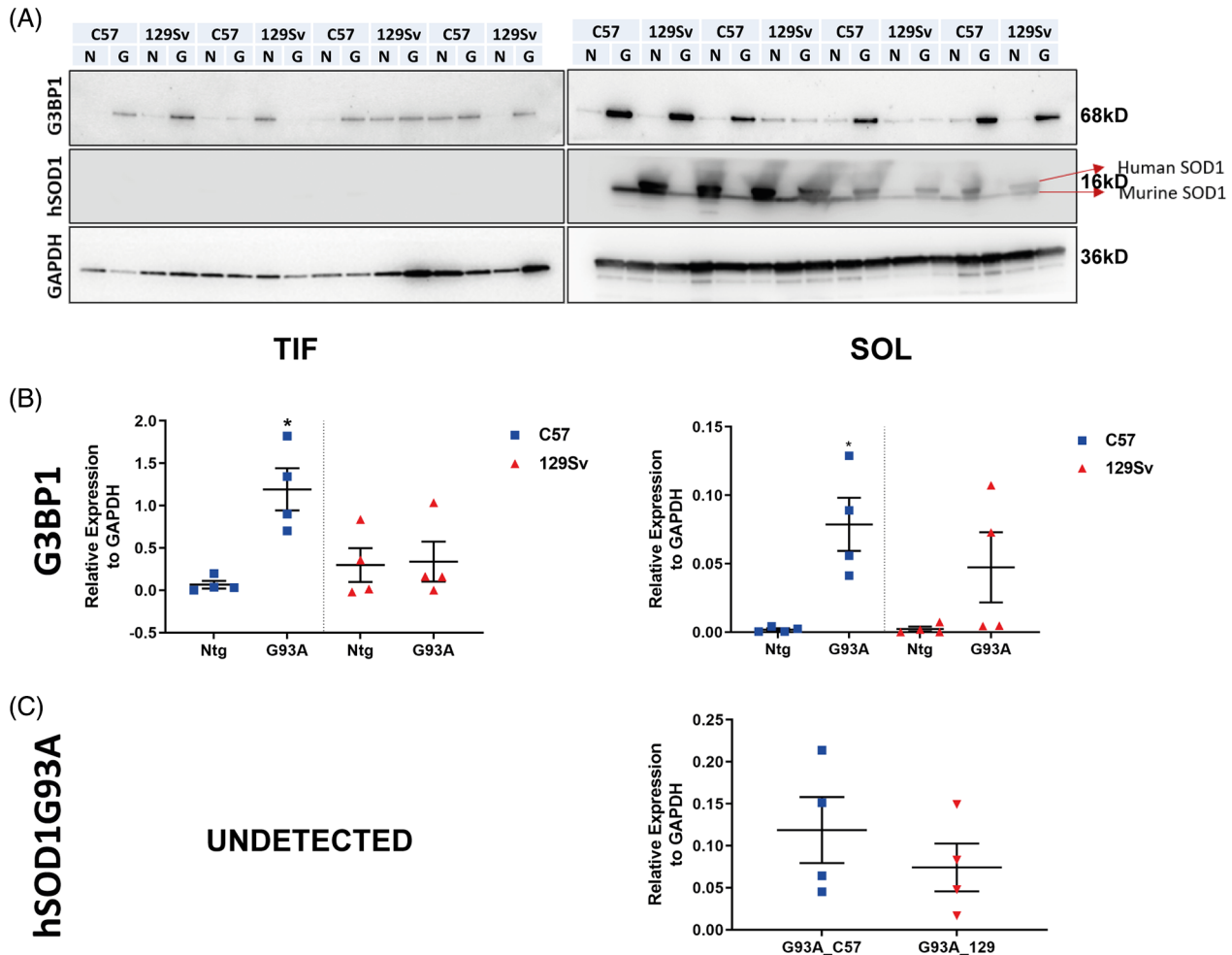
FIGURE 4 Biochemical identification of stress responses in the muscle of fast and slow ALS mouse models. (A–C) Representative immunoblot images and relative densitometric analysis of (A, B) G3BP1 and (A, C) hSOD1 protein expression in TIF and SOL of the TA muscles of C57SOD1G93A and 129SvSOD1G93A mice compared with NTg littermates. Protein levels were normalised on GAPDH expression. Data are reported as mean ± SEM. Significance was calculated for each strain with the unpaired t-test (*$p \leq 0.05$).

muscle, to activate and proliferate. This activation leads to the formation of a transiently amplifying population of myogenic precursor cells (MPCs) that express the Pax7 protein, subsequently followed by the activation of the transcription factor MyoD [24]. Studies have demonstrated the importance of the interactions between the vessels and myogenic cells, besides the supply of oxygen and nutrients. Mainly, endothelial cells (ECs) and MPCs, which are close together, interact to couple myogenesis and angiogenesis during skeletal muscle regeneration [25].

Notably, we found that ANG is expressed by CD31$^+$ capillaries (Figure 5A), blood vessels (Figure 5B) and Pax7$^+$ SCs (Figure 5C) in the skeletal muscle of C57BL6 SOD1G93A mice, suggesting the involvement of the protein in the cross-talk between these cells. Based on this information and the differential ANG expression in the skeletal muscle, we evaluated the extent of vascularisation and muscle regeneration in fast and slow mice during the disease progression. We found increased expression of CD31 by ECs surrounding muscle fibres in the skeletal

muscles of C57_SOD1G93A mice at 12 and 18 weeks of age compared to NTg littermates. Conversely, no increase in CD31 immunostaining was registered in the skeletal muscles of 129Sv_SOD1G93A mice (Figure 5D,E).

We next assessed the involvement of SCs engagement in the skeletal muscle of mice exhibiting fast and slow disease progression rates. Specifically, we examined the protein expression levels of SC-related Pax7 transcription factor [26], in the tibialis anterior (TA) muscle of both fast and slow-progressing mice. Notably, we observed a significant increase in Pax7 protein levels in slow-progressing mice compared to their fast-progressing counterparts at the onset of the disease (Figure 6A,B). Additionally, slow-progressing mice exhibited heightened activation of MyoD (Figure 6A,C), a key factor in determining the final commitment of MPCs to myoblasts [26]. Thus, the early and targeted initiation of myogenesis in slow-progressing mice might contribute to their superior muscle regeneration capabilities. This is supported by the observation of a significantly greater percentage of
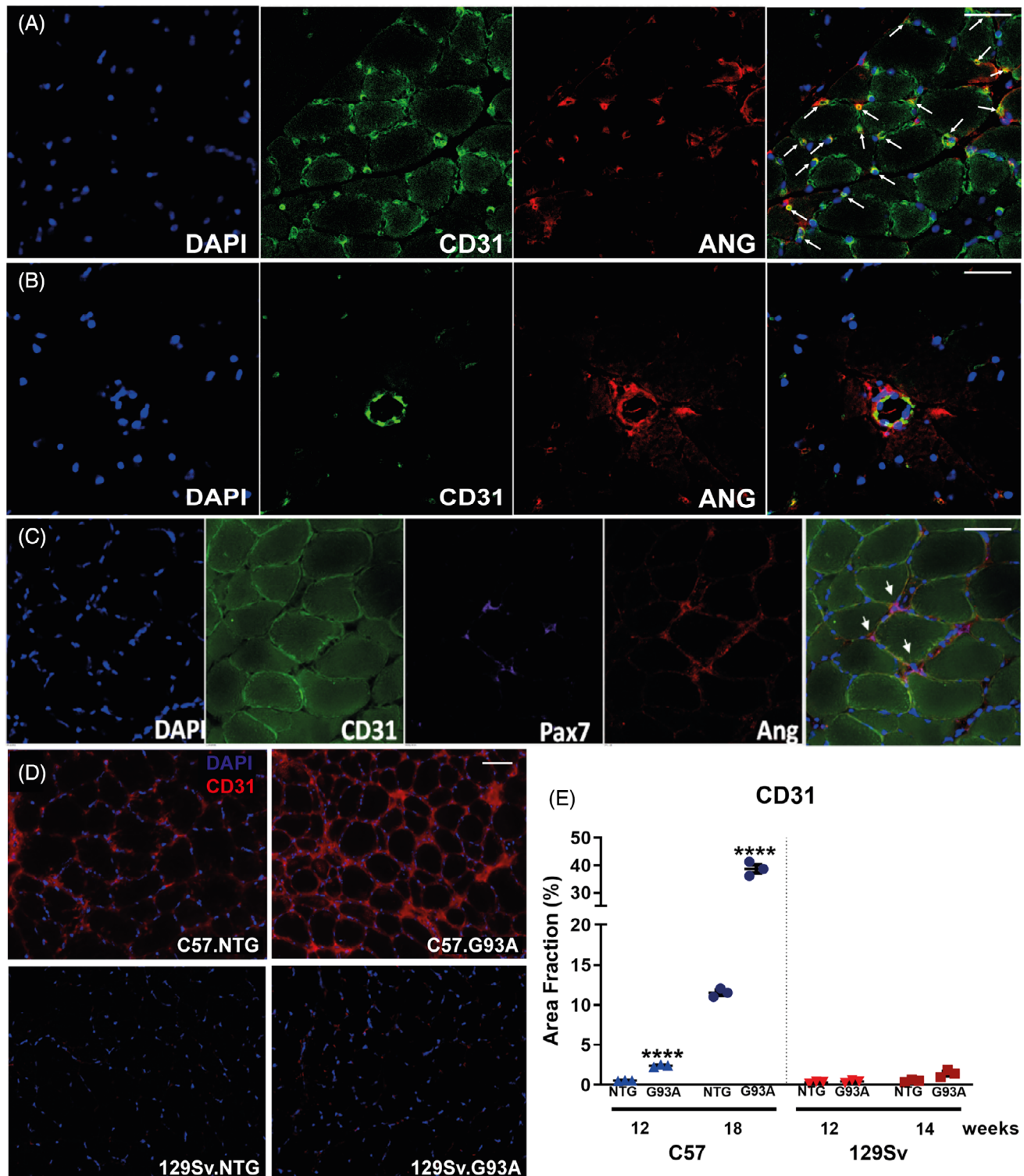
FIGURE 5 Increased Angiogenin protein levels in the skeletal muscle of ALS mice correlates with enhanced muscle vascularisation. (A–C) Representative confocal micrographs showing the signal colocalisation of CD31 (capillaries) and ANG (A), CD31 (vessel) and ANG (B) and Pax7 (satellite cells) and ANG (C) in the skeletal muscle of C57SOD1G93A mice at the disease onset. Scale bars: A–C = 50 μm. (D, E) Representative confocal micrographs and percentage of CD31 coverage area in the TA of fast and slow transgenic mice and relative NTg littermates at the presymptomatic and onset disease stages. Scale bar: 50 μm Data are expressed as the mean ± SEM ($n = 4$). Significance was calculated with one-way ANOVA with uncorrected Fisher's LSD post-analysis (****$p \leq 0.0001$).
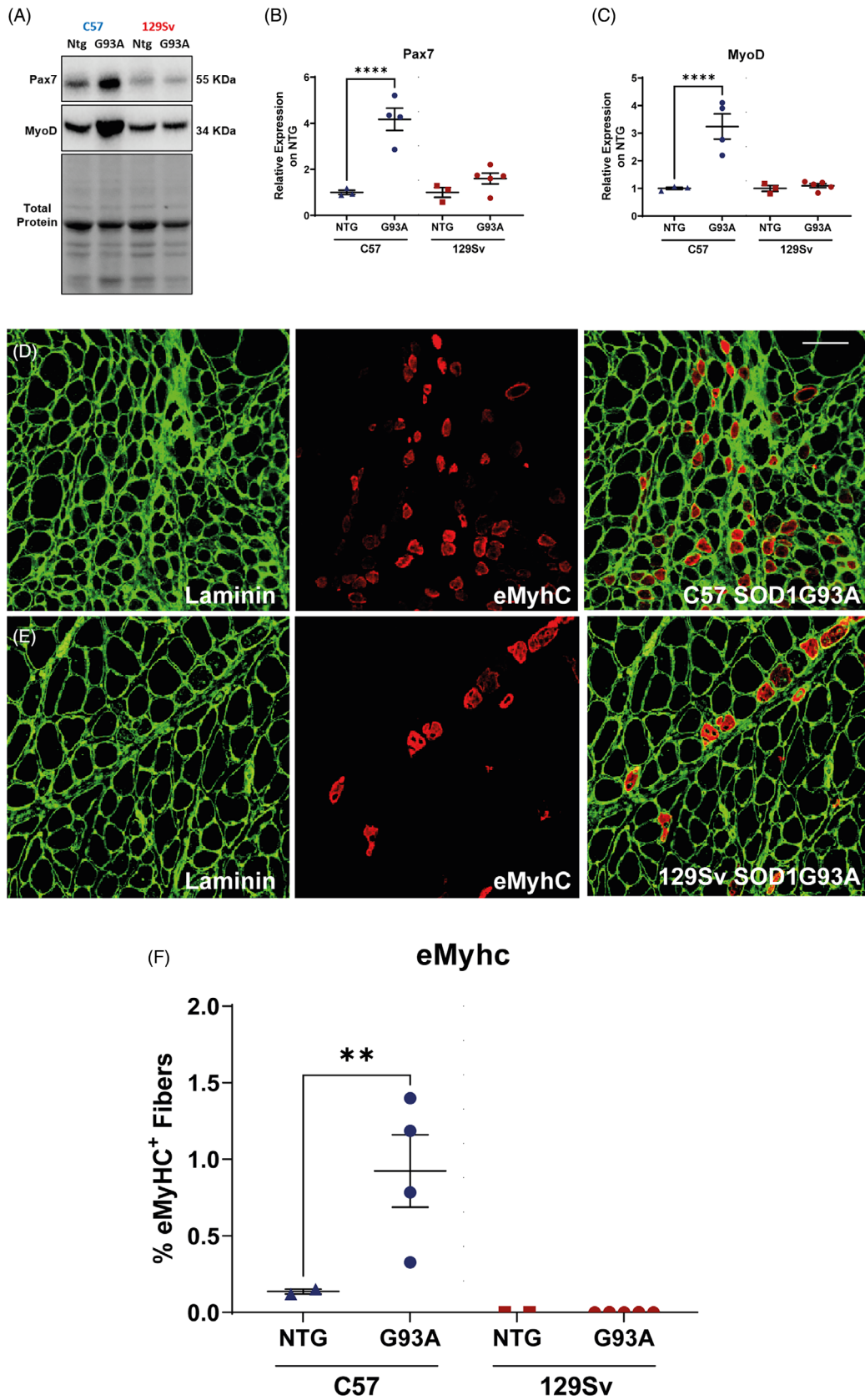
FIGURE 6   Legend on next page.

embryonic (eMyHC$^+$) skeletal muscle fibres in the TA during disease progression, in comparison to mice that exhibit rapid disease progression (Figure 6D,E).

To illustrate that ANG enhances myogenesis, we investigated the direct impact of ANG protein on primary SCs from C57-SOD1G93A mice in vitro. Immunohistochemical staining for the nuclear protein Ki67 indicated an increased proliferation rate in SCs treated with 100 ng/mL of ANG (Figure 7A,B). Additionally, we conducted a differentiation assay on in vitro cultures of SOD1G93A satellite cells to assess ANG ability to enhance their differentiation. After treatment with 100 ng/mL of ANG, SCs displayed an increased differentiation index, as evidenced by a greater percentage of MYHC-positive myocytes compared to the control group (Figure 7C,D). Based on literature showing that ANG-derived tiRNAs promote the differentiation of myoblasts into mature muscle fibres by inhibiting the TGFβ pathway [27], we investigated the effect of ANG treatment on C2C12 murine muscle cell lines. Specifically, we assessed its impact on the phosphorylation of SMAD2/3, key transcription factors in TGFβ signalling [28], and the expression of Pax7 and MyoG, two transcription factors crucial for the SC proliferation and differentiation [26]. Our results showed that ANG effectively inhibits SMAD2/3 phosphorylation (Figure 7E,F) and counteracts the repressive effects of TGFβ on Pax7 (Figure 7E,G) and MyoG expression (Figure 7E,H), supporting the role of ANG in promoting muscle regeneration.

3.4 | Angiogenin is a muscle-prognostic biomarker of ALS

We then conducted a pilot clinical pre-validation study using muscle biopsies from the left Vastus Lateralis of 19 ALS patients, categorised by fast and slow disease progression based on changes in the Functional Rating Scale (ΔFRS) and age-matched at the disease onset (slow progressing patients: 57.8 ± 9.9; fast progressing patients: 58.9 ± 5.4). This study aimed to examine the relationship between ANG protein levels in the muscle and the rate of disease progression by immunoblot (see Supplementary Information). Analysis showed an inverse relationship between ANG expression level in the skeletal muscle and the speed of the disease progression of ALS patients (Figure 8A). Noteworthy, ANG colocalises with both

capillaries (Figure 8B) and blood vessels (Figure 8C) in the muscle tissue of ALS patients with slow disease progression, showing higher CD31 and ANG immunofluorescence staining than those with fast disease progression (Figure 8D). In keeping with our preclinical observations, this finding spotlights ANG as a prognostic biomarker representative of the severity of the disease.

4 | DISCUSSION

In this study, we established the pivotal beneficial role of ANG in skeletal muscle affected by ALS. Notably, we found that a higher protein expression in the skeletal muscles of slow-progressing SOD1G93A mice was associated with increased muscle vascularisation and engagement of myogenic precursor cells towards the differentiation of new myofibres. Interestingly, also in ALS patients, the disease progression exhibited an inverse correlation with the expression level of ANG in skeletal muscle.

Loss-of-function mutations in the ANG gene have been observed in both familial and sporadic ALS cases [6]. Earlier research conducted by our group demonstrated that daily intraperitoneal injections of human ANG (huANG) administered after the onset of symptoms extended lifespan and postponed disease progression in SOD1G93A mice. This effect was noted in MNs, endothelial cells, and the vasculature [7, 9]. ANG is a secreted protein and is known to act in paracrine. For example, MNs secrete ANG during stress conditions and it is taken up by astrocytes and possibly endothelial cells to alter their function to protect MNs [29, 30]. In the present study, we demonstrated that the protective activities of ANG even go beyond CNS function and may involve improved muscle physiology.

Muscle regeneration depends on the ability of SCs, the resident stem cells in muscle, to activate and multiply. This process leads to the emergence of a transiently amplifying population of MPCs that initially express Pax7, followed by the transcription factor MyoD. Subsequently, these MPCs cease cell division, undergo terminal myogenic differentiation, and fuse to create new myofibers [31].

In vivo, SCs are predominantly found adjacent to blood vessels along the myofiber, and there is a strong correlation between the number of capillaries encircling a myofiber and the quantity of SCs associated with that

---

FIGURE 6 Increased Angiogenin protein levels in the skeletal muscle of ALS mice correlates with enhanced myogenesis. (A–C) Representative immunoblot images and relative densitometric analysis of Pax7 (A, B) and MyoD (A, C) protein expression in TA muscles of C57SOD1G93A and 129SvSOD1G93A mice compared with NTg littermates. Protein levels were normalised on the total amount of protein loaded. Data are reported as mean ± SEM. Significance was calculated with Two-way ANOVA with uncorrected Fisher's LSD post-analysis (****$p \leq 0.0001$). (D, E) Representative confocal images of embryonal muscle fibres (eMyHC) on TA coronal sections of C57SOD1G93A (D) and 129SvSOD1G93A (E) mice at onset disease stage, immunostained with laminin. (F) The percentage of embryonal muscle fibres was calculated relative to the total number of fibres in TA muscle and in relation to respective NTg mice. Data are expressed as the mean (±SEM). Significance was calculated with Two-way ANOVA with uncorrected Fisher's LSD post-analysis (**$p \leq 0.01$).
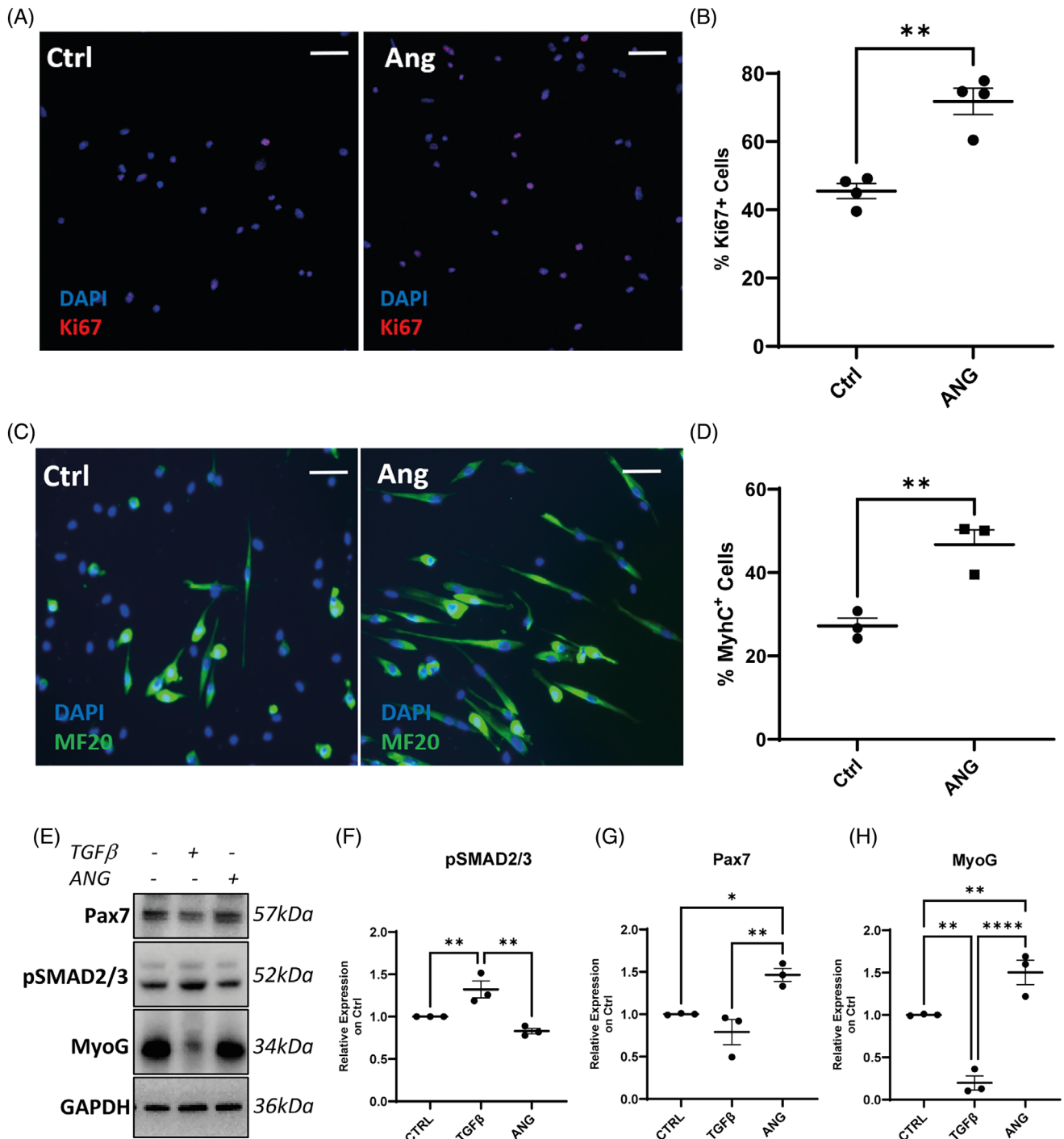
FIGURE 7 In vitro evaluation of satellite cell proliferation and differentiation in the presence of Angiogenin. (A) Representative confocal micrograph showing the immunostaining for Ki67 (red) and DAPI (blue) on primary satellite cell (SC) cultures of C57SOD1G93A mice in growing medium for 72 h treated with Angiogenin or Vehicle for 24 h. Scale bar = 100 μm. (B) The proliferation index was calculated as No. of Ki67 and DAPI positive cells (n = 3). Data are reported by means ± SEM. **p < 0.01 by unpaired t-test. (C) Representative confocal images showing the immunostaining for MF20-MyHC (green) and DAPI (blue) on C57SOD1G93A SCs derived from muscles and cultured in DM for 48 h treated with Angiogenin or Vehicle for 24 h. Scale bar = 50 μm. (D) The fusion index was calculated as (No. nuclei present in MyHC$^+$ cells with two or more nuclei/No. myotubes). Data are reported as the mean ± SEM from three independent experiments for each group. **p < 0.01 by unpaired t-test. (E–H) Representative immunoblot images and relative densitometric analysis of pSMAD2/3 (E, F), Pax7 (E, G) and MyoG (E, H) protein expression in untreated C2C12 muscle cells, treated with TGFβ or ANG. Protein levels were normalised on GAPDH. Data are reported as mean ± SEM of three independent experiments per group. Significance was calculated with One-way ANOVA with uncorrected Fisher's LSD post-analysis (*p ≤ 0.05, **p ≤ 0.01, ****p ≤ 0.0001).
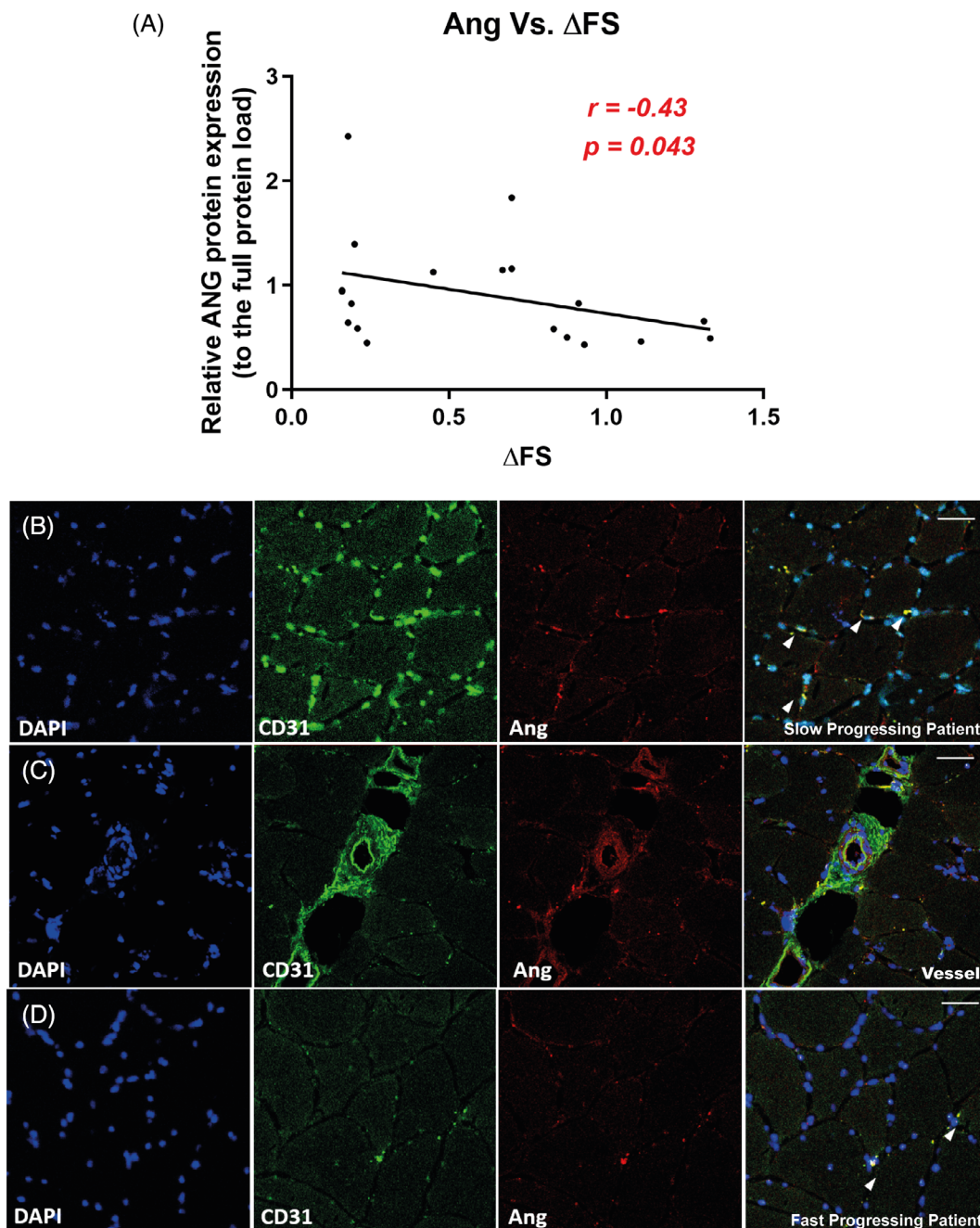
FIGURE 8 The Angiogenin expression correlates with the slow disease progression in sporadic ALS patients. (A) Bivariate analysis showing the strength of association between the muscular protein expression of Angiogenin assessed by immunoblot and the ΔFRS score of ALS patients. The higher is the ΔFRS, the faster is the disease progression. The data were analysed by nonparametric Spearman's rank correlation. (B, D) Representative confocal micrographs showing the signal colocalisation of CD31 (capillaries) and ANG in slow (B) and fast (D) progressing ALS patients. (C) Representative confocal micrograph showing CD31 (vessel) and ANG (C) in slow progressing ALS patient. Scale bars: B–C: 50 μm.

particular myofiber [24]. Extensive research has shown that there are functional interactions between ECs and SCs that support the coupling of myogenesis and angiogenesis during the regeneration of skeletal muscle [25, 32, 33]. These two cell types mutually enhance each other's activity, facilitating both angiogenesis and myogenesis in vivo and in vitro, thus demonstrating the interconnected nature of these biological processes. According to our findings, both SCs and ECs expressed ANG and its expression levels within the skeletal muscle of SOD1G93A were inversely related to the disease severity rate. Indeed, we found an early and specific ANG activation in the TA of slow-progressing mice, and this was associated with greater myogenesis and muscle vascularisation as assessed by an increased percentage of embryonic myofibres and increased capillary density.

Remarkably, this finding has been corroborated in muscle biopsies from patients with sporadic ALS, where it was observed that ANG protein levels inversely correlated with the rate of disease progression. The small noncoding RNAseq analysis on whole skeletal muscle lysates of C57 and 129Sv SOD1G93A mice pinpointed the upregulation of three Ang-derived 5′-tiRNAs – ValCAC, GlyCCC, LysCTT – in the skeletal muscle of slow-progressing mice. 5′-ValCAC was the top-ranked differentially expressed tiRNA fragment in the skeletal muscles of slow-progressing mice. This result mirrors at the periphery what we have recently found in the CNS of ALS mice in which increased ANG in the spinal cord of C57SOD1G93A mice correlated with a rise in the production of the 5′-ValCAC tiRNA at the disease onset [11]. tiRNAs have previously been shown to increase SG formation in neurons [13]. We found that the increase in ANG and tiRNAs was associated with a significant and specific increase of G3BP1 in the insoluble protein fraction compared to NTg mice, suggesting that ANG and tiRNA may trigger a tissue response to increased stress. ANG in the skeletal muscle could, therefore, be added to the list of growth factors, including VEGF and IGF1, that have a pivotal role in the interplay between SCs and ECs during muscle regeneration [25].

ANG and 5′-GlyCCC tiRNA have previously also been shown to be upregulated in injured skeletal muscles [27]. Interestingly, 5′-GlyCCC tiRNA also participated in SC homeostasis. Overexpression of 5′tiRNA-GlyCCC significantly increased expression of Pax7 mRNA and the myogenic differentiation marker MyoD in C2C12 cell lines, and 5′-GlyCCC tiRNA promoted SC activation and myoblast differentiation, accelerating muscle fibre regeneration [27]. Although the precise mechanisms of actions of tiRNAs warrant further investigations, tRNA fragments perform numerous biological functions through varied molecular mechanisms [12]. 5′tiRNA-GlyCCC may influence myogenesis by directly binding to specific mRNAs and regulating their transcription and may utilise the 5′-end seed sequence (evolutionarily conserved fragments on tsRNAs, from the second to the eighth nucleotides) to bind to the 3′UTR of a target gene, thus silencing their expression [27]. In keeping with this, we demonstrated that the exogenous ANG administration to primary SC from SOD1G93A mice elicited their proliferation and differentiation through the inhibition of the TGFβ signalling, leading to the overexpression of promyogenic transcription factors (i.e., Pax7, MyoG). These results describe a novel role of ANG within the skeletal muscles.

Skeletal muscle is among the tissues most profoundly impacted by ALS, and its accessibility via biopsy offers a window into the distal motor system at both earlier stages and in real-time [4, 31]. Skeletal muscle cells are not merely passive recipients of MN signalling for motor function. They actively engage in communication, sending signals to their immediate surroundings, including motor axons, which significantly affects neuromuscular efficiency and may influence MN survival or overall body physiology [31]. Currently, the main focus of ALS research on CNS pathogenic mechanisms has hampered the investigation of peripheral pathophysiology, especially at the muscular level. As a result, there are still few developments in clinical muscle diagnosis. Hitherto, the only suggested muscle tissue biomarker is Nogo-A, which was identified in patients with lower MN disease that progressed to ALS [34]. Besides, plasma creatinine [35], creatine kinase [36] and, more recently, the cardiac troponin T (cTnT) [37, 38] are the only muscle damage by-products tested prospectively as biomarkers with prognostic or diagnostic relevance. In this study, we demonstrate that the skeletal muscle could serve as a paramount source of novel prognostic disease biomarkers. In keeping with preclinical evidence, we found that muscle ANG protein levels were significantly elevated in ALS patients with a less severe phenotype, and this correlated with our published evidence about increased serum 5′-ValCAC tiRNA levels in slow-progressing patients [11].

5 | CONCLUSIONS

This study underscores the crucial role of ANG in peripheral tissues impacted by ALS, especially in skeletal muscle regeneration and vascularisation. The involvement of ANG in the communication between SCs and ECs, possibly facilitated by ANG-generated tiRNAs acting as messenger molecules, highlights its importance in promoting both angiogenesis and myogenesis, ultimately aiding muscle maintenance and function. The identification of ANG-derived tiRNAs as potential indicators for ALS prognosis opens up new avenues for diagnostics, with skeletal muscle emerging as a promising source for novel biomarkers. Future clinical advances could deepen the understanding of the involvement of ANG and its generation of tiRNAs in the progression of ALS, exploiting them as diagnostic indicators and targets for therapy to improve clinical trial results and patient quality of life.

CONFLICT OF INTEREST STATEMENT

The authors declare no conflicts of interest.

DATA AVAILABILITY STATEMENT

All data generated or analysed during this study are included in this published article and its supplementary information files.

ETHICS STATEMENT

All animal studies were conducted in compliance with the ethical standards of the Mario Negri Institute, where the studies took place. Ethical approval for these procedures was granted by the Animal Welfare Office, Department of Public Health and Veterinary, Nutrition and Food Safety, General Management of Animal Care and Veterinary Drugs at the Italian Ministry of Health (protocol number 79/2020PR). Human tissue samples were acquired for diagnostic purposes under a material transfer agreement with the Neuromuscular Bank of Tissues at the University of Padua (Telethon Network of Genetic Biobanks; TNGB), and stored at the Mario Negri biorepositories. Detailed ethical guidelines followed by the Biobank, including aspects of confidentiality/data protection, storage, and distribution of materials, can be found at http://biobanknetwork.telethon.it/Pages/View/TheCharter#ethical_guidelines.

ORCID

Caterina Bendotti https://orcid.org/0000-0003-1055-1271

Jochen H. M. Prehn https://orcid.org/0000-0003-3479-7794

Giovanni Nardo https://orcid.org/0000-0002-1803-1484

REFERENCES

1. Tzeplaeff L, Wilfling S, Requardt MV, Herdick M. Current state and future directions in the therapy of ALS. Cells. 2023;12(11):1523.
2. Kiernan MC, Vucic S, Talbot K, McDermott CJ, Hardiman O, Shefner JM, et al. Improving clinical trial outcomes in amyotrophic lateral sclerosis. Nat Rev Neurol. 2021;17:104–18.
3. Shefner JM, Musaro A, Ngo ST, Lunetta C, Steyn FJ, Robitaille R, et al. Skeletal muscle in amyotrophic lateral sclerosis. Brain. 2023;146:4425–36.
4. Scaricamazza S, Salvatori I, Ferri A, Valle C. Skeletal muscle in ALS: an unappreciated therapeutic opportunity? Cells. 2021;10(3):525.
5. Sheng J, Xu Z. Three decades of research on angiogenin: a review and perspective. Acta Biochim Biophys Sin. 2016;48:399–410.
6. Greenway MJ, Andersen PM, Russ G, Ennis S, Cashman S, Donaghy C, et al. ANG mutations segregate with familial and "sporadic" amyotrophic lateral sclerosis. Nat Genet. 2006;38:411–3.
7. Kieran D, Sebastia J, Greenway MJ, King MA, Connaughton D, Concannon CG, et al. Control of motoneuron survival by angiogenin. J Neurosci. 2008;28:14056–61.
8. Aparicio-Erriu IM, Prehn JHM. Molecular mechanisms in amyotrophic lateral sclerosis: the role of angiogenin, a secreted rnase. Front Neurosci. 2012;6:167.
9. Crivello M, O'Riordan SL, Woods I, Cannon S, Halang L, Coughlan KS, et al. Pleiotropic activity of systemically delivered angiogenin in the SOD1G93A mouse model. Neuropharmacology. 2018;133:503–11.
10. Nardo G, Iennaco R, Fusi N, Heath PR, Marino M, Trolese MC, et al. Transcriptomic indices of fast and slow disease progression in two mouse models of amyotrophic lateral sclerosis. Brain. 2013;136:3305–32.
11. Hogg MC, Rayner M, Susdalzew S, Monsefi N, Crivello M, Woods I, et al. 5'ValCAC tRNA fragment generated as part of a protective angiogenin response provides prognostic value in amyotrophic lateral sclerosis. Brain Commun. 2020;2(2):fcaa138.
12. Fagan SG, Helm M, Prehn JHM. tRNA-derived fragments: a new class of non-coding RNA with key roles in nervous system function and dysfunction. Prog Neurobiol. 2021;205:102118.
13. Emara MM, Ivanov P, Hickman T, Dawra N, Tisdale S, Kedersha N, et al. Angiogenin-induced tRNA-derived stress-induced RNAs promote stress-induced stress granule assembly. J Biol Chem. 2010;285:10959–68.
14. Saikia M, Jobava R, Parisien M, Putnam A, Krokowski D, Gao XH, et al. Angiogenin-cleaved tRNA halves interact with cytochrome c, protecting cells from apoptosis during osmotic stress. Mol Cell Biol. 2014;34:2450–63.
15. Marino M, Papa S, Crippa V, Nardo G, Peviani M, Cheroni C, et al. Differences in protein quality control correlate with phenotype variability in 2 mouse models of familial amyotrophic lateral sclerosis. Neurobiol Aging. 2015;36:492–504.
16. Margotta C, Fabbrizio P, Ceccanti M, Cambieri C, Rufolo G, D'Agostino J, et al. Immune-mediated myogenesis and acetylcholine receptor clustering promote a slow disease progression in ALS mouse models. Inflamm Regen. 2023;43(1):25.
17. Donovan PD, McHale NM, Venø MT, Prehn JHM. tsRNAsearch: a pipeline for the identification of tRNA and ncRNA fragments from small RNA-sequencing data. Bioinformatics. 2021;37:4424–30.
18. Kimura F, Fujimura C, Ishida S, Nakajima H, Furutama D, Uehara H, et al. Progression rate of ALSFRS-R at time of diagnosis predicts survival time in ALS. Neurology. 2006;66:265–7.
19. Basso M, Samengo G, Nardo G, Massignan T, D'Alessandro G, Tartari S, et al. Characterization of detergent-insoluble proteins in ALS indicates a causal link between nitrative stress and aggregation in pathogenesis. PLoS One. 2009;4(12):e8130.
20. Fabbrizio P, D'Agostino J, Margotta C, Mella G, Panini N, Pasetto L, et al. Contingent intramuscular boosting of P2XR7 axis

improves motor function in transgenic ALS mice. Cell Mol Life Sci. 2022;79:7.

21. Verma S, Khurana S, Vats A, Sahu B, Ganguly NK, Chakraborti P, et al. Neuromuscular junction dysfunction in amyotrophic lateral sclerosis. Mol Neurobiol. 2022;59:1502–27.

22. Wolozin B. Regulated protein aggregation: stress granules and neurodegeneration. Mol Neurodegener. 2012;7:56.

23. Wei R, Bhattacharya A, Chintalaramulu N, Jernigan AL, Liu Y, van Remmen H. Protein misfolding, mitochondrial dysfunction and muscle loss are not directly dependent on soluble and aggregation state of mSOD1 protein in skeletal muscle of ALS. Biochem Biophys Res Commun. 2012;417:1275–9.

24. Chiristov C, Chrétien F, Abou-Khalil R, Bassez G, Vallet G, Authier F-J, et al. Muscle satellite cells and endothelial cells: close neighbors and privileged partners. Mol Biol Cell. 2007;18:1397–409.

25. Latroche C, Weiss-Gayet M, Muller L, Gitiaux C, Leblanc P, Liot S, et al. Coupling between Myogenesis and angiogenesis during skeletal muscle regeneration is stimulated by restorative macrophages. Stem Cell Reports. 2017;9:2018–33.

26. Musarò A. The basis of muscle regeneration. Adv Biol. 2014;2014:1–16.

27. Shen L, Liao T, Chen Q, Lei Y, Wang L, Gu H, et al. tRNA-derived small RNA, 5'tiRNA-Gly-CCC, promotes skeletal muscle regeneration through the inflammatory response. J Cachexia Sarcopenia Muscle. 2023;14:1033–45.

28. Nakao A, Imamura T, Souchelnytskyi S, Kawabata M, Ishisaki A, Oeda E, et al. TGF-beta receptor-mediated signalling through Smad2, Smad3 and Smad4. EMBO J. 1997;16:5353–62.

29. Skorupa A, Urbach S, Vigy O, King MA, Chaumont-Dubel S, Prehn JHM, et al. Angiogenin induces modifications in the astrocyte secretome: relevance to amyotrophic lateral sclerosis. J Proteomics. 2013;91:274–85.

30. Skorupa A, King MA, Aparicio IM, Dussmann H, Coughlan K, Breen B, et al. Motoneurons secrete angiogenin to induce RNA cleavage in astroglia. J Neurosci. 2012;32:5024–38.

31. Manzano R, Toivonen JM, Moreno-Martínez L, de la Torre M, Moreno-García L, López-Royo T, et al. What skeletal muscle has to say in amyotrophic lateral sclerosis: implications for therapy. Br J Pharmacol. 2021;178:1279–97.

32. Borselli C, Storrie H, Benesch-Lee F, Shvartsman D, Cezar C, Lichtman JW, et al. Functional muscle regeneration with combined delivery of angiogenesis and myogenesis factors. Proc Natl Acad Sci U S A. 2010;107:3287–92.

33. Verma M, Asakura Y, Murakonda BSR, Pengo T, Latroche C, Chazaud B, et al. Muscle satellite cell cross-talk with a vascular niche maintains quiescence via VEGF and notch signaling. Cell Stem Cell. 2018;23:530–543.e9.

34. Dupuis L, Gonzalez de Aguilar JL, Di Scala F, Rene F, de Tapia M, Pradat P-F, et al. Nogo provides a molecular marker for diagnosis of amyotrophic lateral sclerosis. Neurobiol Dis. 2002;10:358–65.

35. Liu J, Luo X, Chen X, Shang H. Serum creatinine levels in patients with amyotrophic lateral sclerosis: a systematic review and meta-analysis. Amyotroph Lateral Scler Frontotemporal Degener. 2020;21:502–8.

36. Ceccanti M, Pozzilli V, Cambieri C, Libonati L, Onesti E, Frasca V, et al. Creatine kinase and progression rate in amyotrophic lateral sclerosis. Cells. 2020;9:1174.

37. Castro-Gomez S, Radermacher B, Tacik P, Mirandola SR, Heneka MT, Weydt P. Teaching an old dog new tricks: serum troponin T as a biomarker in amyotrophic lateral sclerosis. Brain Commun. 2021;3(4):fcab274.

38. Kläppe U, Chamoun S, Shen Q, Finn A, Evertsson B, Zetterberg H, et al. Cardiac troponin T is elevated and increases longitudinally in ALS patients. Amyotroph Lateral Scler Frontotemporal Degener. 2022;23:58–65.

SUPPORTING INFORMATION

Additional supporting information can be found online in the Supporting Information section at the end of this article.

How to cite this article: Fabbrizio P, Baindoor S, Margotta C, Su J, Morrissey EP, Woods I, et al. Protective role of Angiogenin in muscle regeneration in amyotrophic lateral sclerosis: Diagnostic and therapeutic implications. Brain Pathology. 2024. e13328. https://doi.org/10.1111/bpa.13328